Comparison of thyristor and insulated-gate bipolar transistor -based power supply topologies in industrial water electrolysis applications

Koponen Joonas, Poluektov Anton, Ruuskanen Vesa, Kosonen Antti, Niemelä Markku, Ahola Jero

DOI: 10.1016/j.jpowsour.2020.229443

Comparison of thyristor and insulated-gate bipolar transistor -based power supply topologies in industrial water electrolysis applications

Joonas Koponen[a,*], Anton Poluektov[a], Vesa Ruuskanen[a], Antti Kosonen[a], Markku Niemelä[a], Jero Ahola[a]

[a]*LUT University, P.O. Box 20, FI-53851, Lappeenranta, Finland*

Abstract

The demand for green hydrogen is growing as the increasing production of pure hydrogen can no longer be based on fossil hydrocarbons. As water electrolysis would move from niche to a significant consumer of emission-free electricity, the efficiency of electrolytic gas production, lifetime of water electrolysis systems, and balance in the electricity grid become essential. The operational and investment costs of an industrial-scale alkaline water electrolyzer with four practical rectifier topologies are investigated. The results show thyristor-based rectifiers provide poor quality for the AC and DC sides, which leads to nonoptimal specific energy consumption (SEC) of the water electrolyzer and a notable reactive power component. Transistor-based topologies may offer up to 4.5% lower SEC of the electrolyzer than the conventional 6-pulse thyristor bridge. The reactive power results in additional costs in either investments in compensation equipment or regular allowance costs. An additional DC/DC converter can be installed to im-

*Corresponding author, joonas.k.koponen@lut.fi, tel. +358-50-563-6569

prove the power quality for the electrolyzer, but the second conversion stage adds to the system complexity and cost without eliminating reactive power. A modular single-stage rectifier based on insulated-gate bipolar transistor (IGBT) bridges is suggested as an alternative to provide improved power quality for both the electrolyzer and the electricity grid.
Keywords: Water electrolysis, Energy conversion, Specific energy consumption, Power quality, Power supply.

1. Introduction

Annual carbon dioxide emissions of the world economy should reach at least a net zero level by 2050 to limit the global temperature rise well below 2 °C [1]. Wider deployment of renewable energy generators requires cost-effective systems for storing intermittently generated electrical energy and supporting power systems. In regions with large renewable power production capacities, the issue of curtailed power is more acute and Power-to-Gas systems are considered feasible [2, 3, 4, 5]. However, transforming only the electricity production into emission-free power sources is not enough as the transportation, industrial, and agricultural sectors are also significant contributors to the CO_2 emissions. Cement, chemical, iron, and steel industries are the largest industrial fossil CO_2 emitters. Bridges between the different energy use sectors are needed to create a connection to emission-free electrical energy sources. To this end, hydrogen is one of the possible energy vectors.

Water electrolysis is a process where water molecules are split into hydrogen (H_2) and oxygen (O_2) with the aid of electric current. A majority of

the electrical energy supplied to water electrolysis is carried as the chemical energy of hydrogen as water electrolyzer efficiencies exceeding 80%—based on the higher heating value (HHV) of hydrogen—are achievable with commercial technologies [6]. Water electrolysis is feasible for industrial-scale production of hydrogen and can transfer emission-free electrical energy to the production of carbon-neutral fuels, raw materials, and chemicals in the hydrogen required to form the constituent synthetic compounds. Hydrogen can also be used directly to enable the defossilization of key industrial processes, such as steel manufacturing. The global energy transformation may require terawatts of installed water electrolyzer capacity by 2050 to provide the required green hydrogen [7, 8]. In the more near term, the EU has set a target to have 40 GW of water electrolysis capacity installed within the EU area and another 40 GW installed within the adjacent countries by 2030 [9].

A life cycle assessment of commercially available electrolyzer technologies is given in [10]. Despite the different materials used, the difference in the environmental footprint left by different electrolyzers becomes less significant when their performance during hydrogen production is evaluated. For each studied technology, electricity consumption accounts for $\geq$90 % of the overall impact. Optimizing the SEC, lifetime, and cost of water electrolyzer systems may have a significant effect on the future world economy.

Rectification is required to execute controlled power consumption in water electrolyzer systems connected to the main AC electricity grid as water electrolyzers are current-controlled DC loads. Industrial water electrolyzers are characterized by high DC currents and relatively low voltages, and rectifiers based on thyristors and diodes have been most common in high-power appli-

cations [11, 12]. The rectifier is responsible for energy efficient and safe power consumption in water electrolyzers based on the operating temperature, pressure, and current density of the electrolytic cell stack. Taking into account the role of the rectifier in the energy efficiency of the water electrolyzer different power supply approaches have been compared [13, 14, 15, 16]. Improved power quality by transistor-based power supplies has been reported to be able to decrease the electrical energy consumption of alkaline water electrolyzers by up to 13% [15, 16] compared to conventional thyristor-based power supplies. Furthermore, smart grid environment simulations have shown a 15% cost decrease potential for the price of electrolytic hydrogen with transistor-based topologies due to higher efficiency in electrolysis and increased operating hours enabled by the wider load range achievable with improved DC power quality [17]. However, capital expenditures (CAPEX) of the rectifier topologies and reactive power compensation were excluded from these previous studies.

The natural commutation of the thyristors produces significant harmonics to the supplied DC current and DC voltage, which causes additional heat losses and imposes a constant dynamic operation on the electrolytic cell stack [15]. The harmonics produced by the thyristors can be costly to filter out because of their low frequency and high amplitude. Furthermore, the thyristor operation causes a flow of reactive power, which varies as a function of the water electrolyzer load current. The reactive power must be compensated for by using additional equipment on the AC side, such as a distribution static compensator (DSTATCOM) and/or passive filters, which increase the CAPEX of the overall system [18]. The power factor may require significant

compensation especially in partial load water electrolyzer operation [19].

In this paper, four practical rectifier topologies are considered for a 3 MW water electrolyzer application in terms of the SEC of the water electrolyzer stack and additionally the CAPEX of the overall system; 1) 6-pulse thyristor bridge, 2) 12-pulse thyristor rectifier bridge, 3) 12-pulse diode bridge followed by an IGBT buck converter, and 4) a modular single-stage IGBT rectifier. The investigation adds a transformer model to the simulation model discussed in [19], and uses a more accurate model for the power supply and the water electrolyzer stack than previously presented by the authors in [15]. SEC analysis includes only the DC current and voltage waveforms created by the four power supply topologies. CAPEX and operational expenditures (OPEX) analyses include also the contribution of reactive power compensation. A novel single-stage IGBT bridge rectifier solution is presented for electrolysis applications as a more modern alternative. Real drive cycle data from an industrial alkaline water electrolysis plant are used in the analysis to compare the annual energy consumptions with the four power supply topologies under study.

This paper is organized as follows. Section 2 introduces the research methods, the simulation model approach, the definitions for the SEC of water electrolysis, and the definitions for electrical power. Section 3 presents the simulation results and a discussion for the CAPEX and OPEX of the power supply configurations considered for industrial water electrolysis applications. Section 4 concludes the paper.

2. Materials and methods

The simulation models to compare different power supply topologies in industrial water electrolysis applications are implemented in MATLAB and Simulink using Simscape Power Systems and Simscape Electrical libraries. The current–voltage characteristic curve of the industrial 3 MW alkaline water electrolyzer used in the simulations of this study is presented in Fig. 1e. The electrolytic cell stack is implemented in the Simulink model as a variable resistor from the Simscape library preceded by a 1 µF capacitor to add capacitive behaviour to the electrolytic cell stack—the double-layer capacitance of a single electrolytic cell may be higher, but adding capacitors in series (bipolar stack) results in a reciprocal of the sum of the reciprocals of each double-layer capacitance. The modelled equivalent stack resistance value is selected based on the instantaneous stack electric current using an interpolating lookup table, whose output is an input for the variable resistor block in Simscape. The AC supply from the 20 kV grid, transformers, rectifiers, possible filters, and DC current control are included. The simulated rectifier topologies are illustrated in Fig. 1. Fig. 1a and Fig. 1b represent the most common solution for AC to DC conversion in high-power, high-current applications [12]. Fig. 1c is a commercial two-stage alternative, where an IGBT buck converter—also called a step-down converter or a chopper circuit—is installed in series after the thyristor and/or diode bridge. The number of parallel IGBT switches in the buck converter must be high enough to limit the current for a single switch low enough to be safely managed. The fourth topology (Fig. 1d) uses parallel IGBT modules similar to power electronic converters in wind turbines, centralized solar photovoltaic (PV) systems or

grid-connected batteries. The forced commutation bidirectional switches of the converter modules can in the future be based on silicon carbide (SiC) and/or gallium nitride (GaN) instead of the silicon IGBTs.

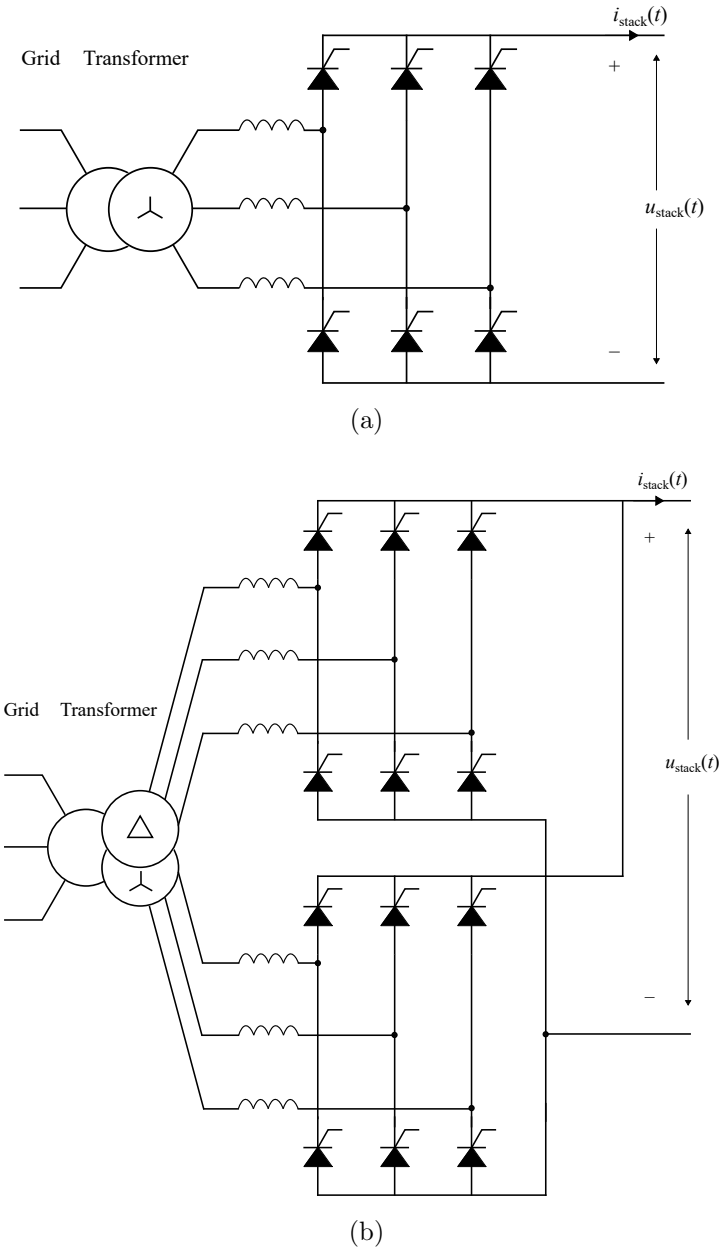

Fig. 1. Rectifier topologies applied to the Simulink simulations, and the applied current–voltage characteristics of the industrial 3 MW alkaline water electrolyzer; (a) 6-pulse thyristor bridge, (b) 12-pulse thyristor rectifier bridge

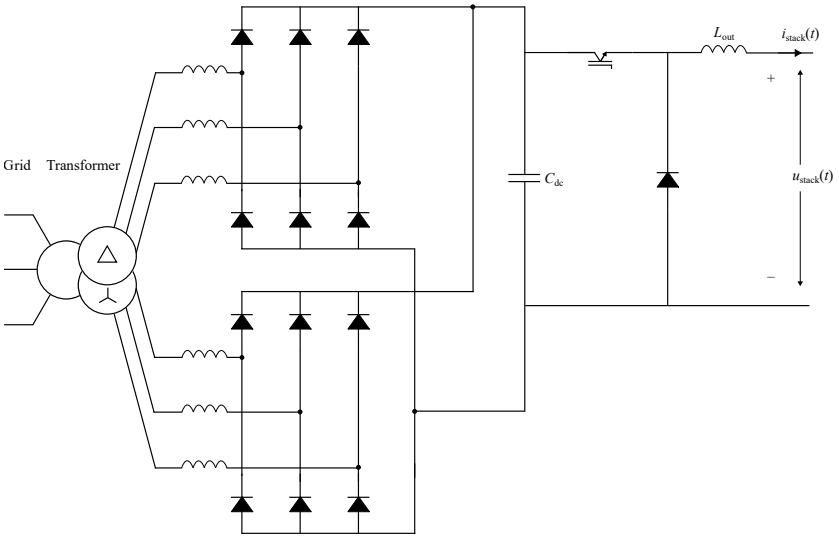

(c)

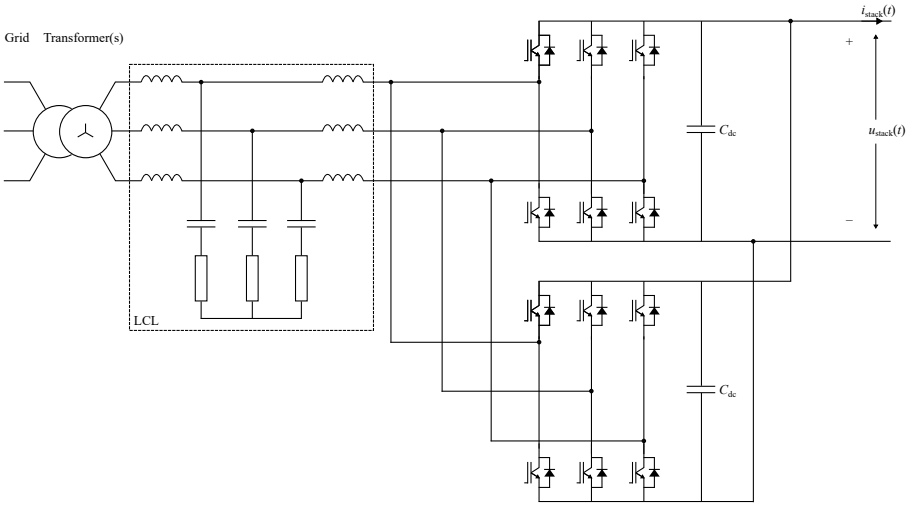

(d)

Fig. 1. (continued) (c) 12-pulse diode bridge followed by an IGBT buck converter, (d) modular single-stage IGBT rectifier, where, for the 3 MW case, the solution consists of five LCL filters and a total of ten bidirectional IGBT bridges

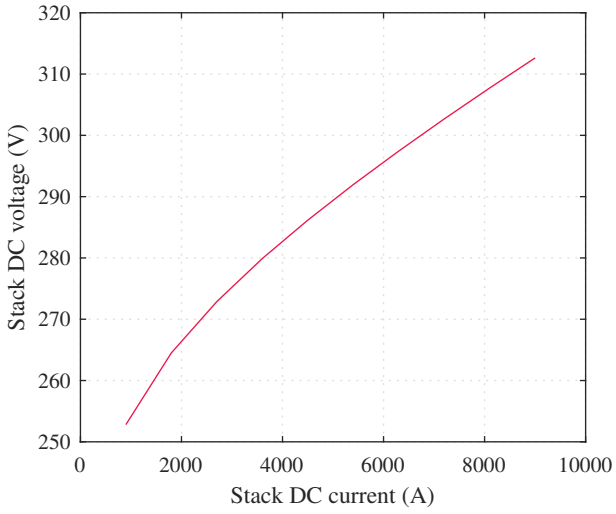

(e)

Fig. 1. (continued) (e) applied polarization curve.

2.1. Design of the modular single-stage IGBT rectifier

The novel modular topology presented in Fig. 1d is configured in the Simulink model to comprise five LCL filters with two two-level bidirectional IGBT converter bridges behind each LCL filter to supply the 3 MW alkaline water electrolyzer. The topology is voltage-boosting and the DC output voltage is at least $\sqrt{2}$ times the root mean square (RMS) value of the line-to-line AC voltage. The LCL filter design for the modular topology follows [20]. Each of the ten parallel pulse-width modulation (PWM) controlled IGBT modules receives the measured instantaneous three-phase AC voltage and current, the fundamental component of the three-phase signal phase, the DC voltage, and the DC voltage set point as inputs to control the DC voltage and the current i_{d} and i_{q} components in unison. To eliminate circulating currents, the IGBT bridge pairs sharing a common LCL filter have identical

pulse signals. In the case of differing pulse signals for the IGBT bridges, when DC buses are common for all the IGBT converter modules, the AC sides should be galvanically isolated between the supply modules. Otherwise, without galvanic isolation on the AC side, the circulating currents would have to be taken into account for example in the current control [21], 60° clamping in space-vector modulation [22], or common-mode coil design [23].

2.2. Specific energy consumption

Hydrogen production rate ($\mathrm{mol\,s^{-1}}$) of an electrolytic cell is linearly proportional to the electric current

$$\dot{n}_{\mathrm{H_2}} = \eta_{\mathrm{F}} \frac{I_{\mathrm{cell,mean}}}{zF}, \tag{1}$$

where $\dot{n}_{\mathrm{H_2}}$ is the hydrogen production rate ($\mathrm{mol\,s^{-1}}$), η_{F} is the effective Faradaic efficiency, also known as the current efficiency, z is the number of moles of electrons transferred in the reaction (for hydrogen, $z = 2$ as water is reduced to hydrogen, i.e., each hydrogen atom gains an electron), F is the Faraday constant ($9.6485 \times 10^4\,\mathrm{C\,mol^{-1}}$), and $I_{\mathrm{cell,mean}}$ is the mean value of stack current (A). In this study, the Faradaic efficiency is assumed to be 100% at all times for the electrolytic cell stack. In practice, Faradaic efficiency has the lowest values at the lowest current densities, and therefore the effective hydrogen production of an electrolytic cell may be decreased under relatively high current ripple amplitude.

The SEC of an electrolyzer can be calculated based on the instantaneous stack voltage, instantaneous stack current, and hydrogen production rate

$$E_{\mathrm{s}} = \frac{\int_0^{t_1} i(t)\, u(t) \mathrm{d}t}{\int_0^{t_1} \dot{m}_{\mathrm{H_2}} \mathrm{d}t}, \tag{2}$$

where E_{s} is the SEC, $i(t)$ is the instantaneous stack current, $u(t)$ is the instantaneous stack voltage, $\dot{m}_{\mathrm{H_2}}$ is the hydrogen gas mass flow rate, and t_1 is the time span under study. Using corresponding units, the HHV of hydrogen gas is 39.4 kWh/kg, the reference SEC level for energy efficiency calculations. Resistive power loss in an electrical conductor or load is directly proportional to the square of the electric current. An instantaneous increase in electric current strongly contributes to the resistive power loss because of the quadratic relationship between the electric current and the resistive power loss. In an electrolytic cell, in addition to the ohmic overpotential, power is consumed in activation overpotential caused by electrode kinetics. The activation overpotential is not linearly proportional to the electric current, which results in slightly decreasing cell voltage mean value with increasing sinusoidal current ripple, while the cell voltage RMS is affected by the dominating—linear or nonlinear—loss region of the electrolytic cell [24]. The greater the current ripple in the DC current for an electrolyzer, the greater is the difference between the RMS and mean values of the DC current. Therefore, DC current ripple should be minimized to reduce losses in water electrolysis processes. Furthermore, the current ripple imposes a dynamic operation on a millisecond time scale for the electrolyzer, which may accelerate degradation of the electrolytic cells. The SEC values presented in this paper consider only the DC current and voltage waveforms created by the power supply topologies.

2.3. Definitions for electric power

Instantaneous power is the product of instantaneous voltage and current values, and active power is the mean value of instantaneous power. In addition to the active power flow, the reactive power components are analyzed for each rectifier topology according to [19]. In a complex presentation, the relation of the apparent power S, the active power P, and the reactive power Q is

$$S^2 = P^2 + Q^2. \tag{3}$$

From Eq. 3, the power factor $\cos\phi$ is defined as

$$\cos\phi = \frac{P}{S}. \tag{4}$$

The apparent power is

$$S = U\,I, \tag{5}$$

where U is the RMS value of voltage, and I is the RMS value of current. Reactive power can be further divided into

$$Q^2 = Q_{\mathrm{S}}^2 + Q_{\mathrm{D}}^2, \tag{6}$$

where Q_{S} is the phase shift component, and Q_{D} is the distortion component of the reactive power. The phase shift component of reactive power is defined by the sum of frequency components, which are often defined by a discrete Fourier transform (DFT) describing the signal as a sum of sinusoidal frequency components, i.e., harmonics, as

	Stack power of nominal (%)									
	0–10%	10–20%	20–30%	30–40%	40–50%	50–60%	60–70%	70–80%	80–90%	90–100%
(a) Grid profile, proportion (%)	9.1	2.4	2.1	2.2	2.2	2.7	6.4	17.6	32.3	23.0
(b) Estimated profile, proportion (%)	22.6	19.1	16.1	13.1	10.1	8.9	5.4	3.0	1.2	0.6

Table 1. Distribution of operating the water electrolyzer at various loads in two alternative cases. The load of nominal is referenced to 9000 A DC current for the 3 MW water electrolyzer. (a) Real load distribution profile in industrial use. (b) Estimated load distribution profile when a high share of intermittent renewable power production is present in the electricity grid.

$$Q_{\mathrm{S}} = \sum_{h=1}^{v} U_h \, I_h \, \sin\theta_h, \tag{7}$$

where v is the number of harmonic components, U_h is the voltage RMS value of the respective harmonic, I_h is the current RMS value of the respective harmonic, and θ_h is the phase shift angle of the respective voltage and current harmonics.

2.4. Drive cycle of the industrial water electrolyzer

A simulation of the electrolyzer operation with the four different power supply topologies is conducted to analyze the energy consumption of the electrolyzer in actual industrial use (load profile (a) in Table 1), and in hypothetical use when intermittent renewable power production is prevalent in the energy system (load profile (b) in Table 1) [2]. For the year under consideration, 9% of the year the real industrial water electrolyzer is not in use, and the total annual electrical energy consumption for the stack is 18.6 GWh.

3. Results and discussion

3.1. Simulated 6-pulse thyristor bridge

The 6-pulse thyristor bridge is connected to the 20 kV, 50 Hz electricity grid through a 3.9 MVA two-winding three-phase transformer, whose resistance and leakage inductance are set to 0.2% and 6%, respectively, for both windings. In SI units, the leakage inductance for the secondary winding is 3.1 µH. The magnetization resistance and the magnetization inductance are left to their default Simulink values, 500 pu. Transformer saturation is not simulated. Grounded Y is selected for both winding connections for measurement purposes. In practice, delta connection is more typical on the medium voltage power distribution. The line-to-line voltage RMS value of the transformer secondary winding is set to 250 V. A single proportional–integral–derivative (PID) controller Simulink block controls the firing angle of the thyristors to supply the desired DC current to the 3 MW water electrolyzer stack. The resulting AC and DC voltage and current waveforms with the 6-pulse thyristor bridge at 9000 A and 1000 A DC current set points are presented in Fig. 2. The DC current and DC voltage waveforms show a significant 300 Hz harmonic component caused by the six natural commutation thyristor switches in the 50 Hz electricity grid. The 1000 A DC current set point may be unsafe with the 6-pulse thyristor bridge as the instantaneous DC current gets very close to zero, 1.2 A at the minimum (Fig. 2c), and an increased amount of time is spent at current densities where gas crossover phenomena have a relatively higher contribution to the electrolytic gas production. Meanwhile, the AC waveforms reveal a significant mismatch between the current and voltage waveforms, which indicates a flow of reactive

power. The simulated 6-pulse thyristor bridge current and voltage waveforms are compared with actual industrial waveforms in Fig. 3.

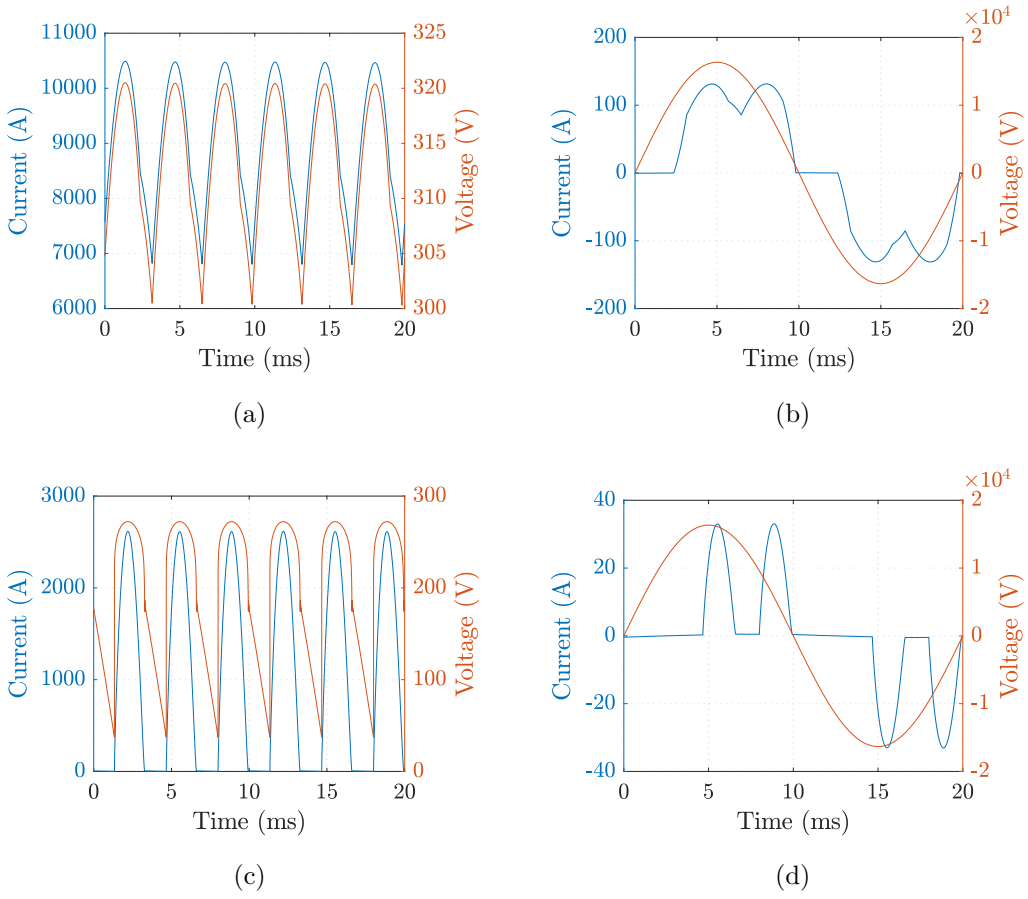

Fig. 2. Current and voltage waveforms as a function of time with the 6-pulse thyristor rectifier; (a) electrolyzer side $I_{\mathrm{DC}} = 9000\,\mathrm{A}$, (b) AC side $I_{\mathrm{DC}} = 9000\,\mathrm{A}$, (c) electrolyzer side $I_{\mathrm{DC}} = 1000\,\mathrm{A}$, (d) AC side $I_{\mathrm{DC}} = 1000\,\mathrm{A}$.

3.2. Simulated 12-pulse thyristor bridge

The 12-pulse thyristor bridge is connected to the 20 kV, 50 Hz electricity grid through a 3.9 MVA three-winding three-phase transformer, whose

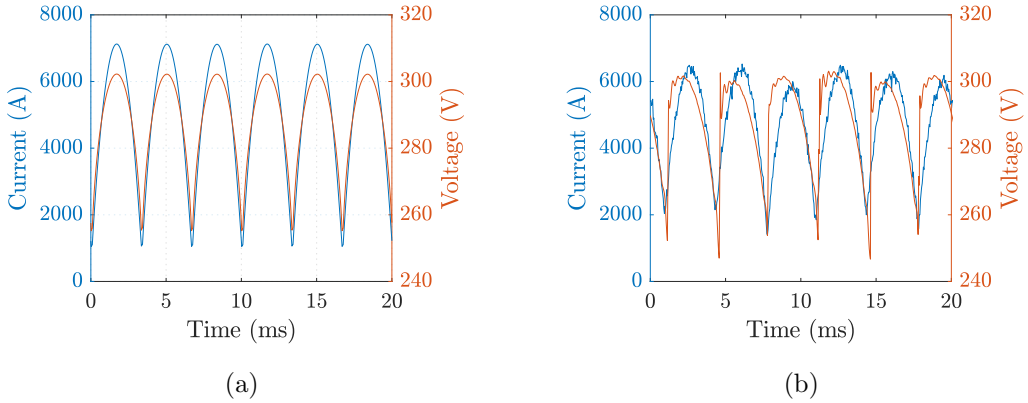

Fig. 3. Current and voltage waveforms as a function of time with the 6-pulse thyristor rectifier compared with measured industrial values; (a) simulated $I_{\mathrm{DC}} = 5000\,\mathrm{A}$, (b) measured $I_{\mathrm{DC}} = 4730\,\mathrm{A}$.

resistance and leakage inductance are set to 0.2% and 6%, respectively, for each winding. Starting from the primary, the winding connections of the transformer are set to grounded Y, grounded Y, and delta (D1). The line-to-line voltage RMS value of the transformer secondary windings is set to 250 V. The resulting AC and DC voltage and current waveforms with the 12-pulse thyristor bridge at the 9000 A and 1000 A DC current set points are presented in Fig. 4. The DC current and DC voltage waveforms show a significant 600 Hz harmonic component caused by the 12 natural commutation thyristor switches in the 50 Hz electricity grid. The 1000 A DC current set point may be unsafe with the 12-pulse thyristor bridge as the instantaneous DC current approaches zero, 5.6 A at the minimum (Fig. 4c). At the nominal 9000 A DC current set point, the AC current and AC voltage waveforms match each other more closely with the 12-pulse thyristor topology than with the 6-pulse thyristor topology.

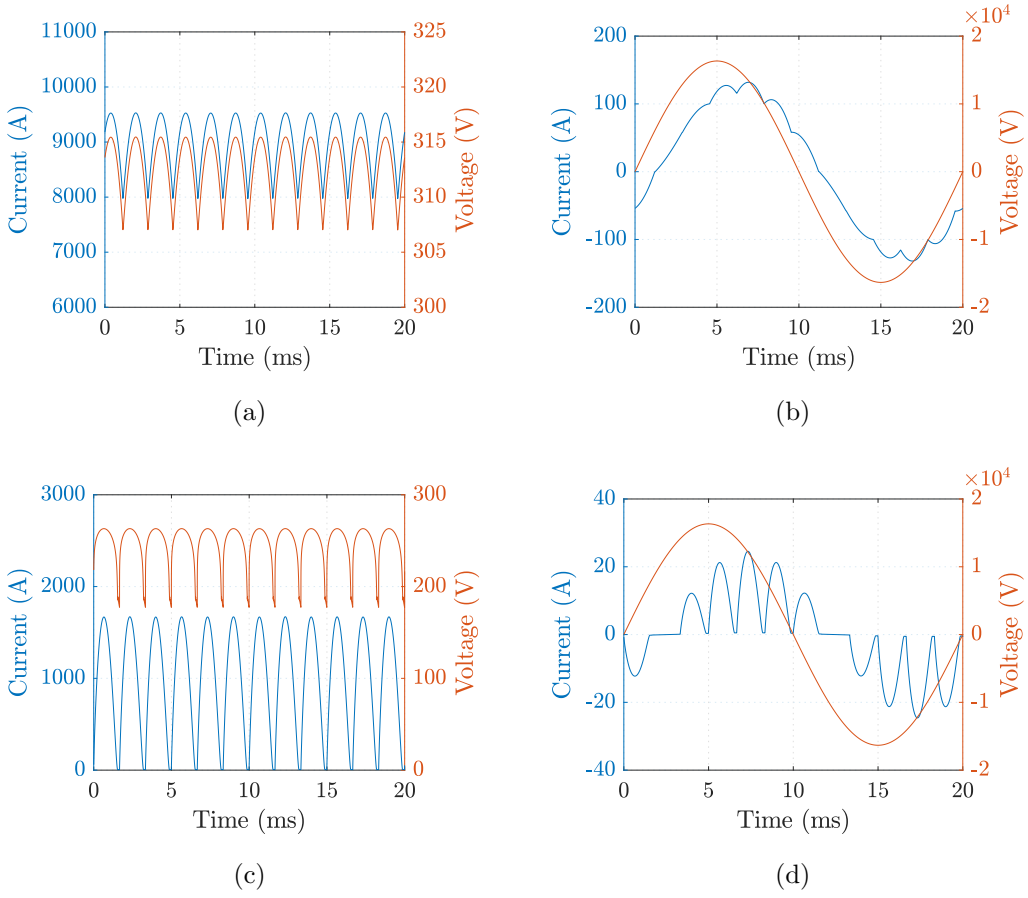

Fig. 4. Current and voltage waveforms as a function of time with the 12-pulse thyristor rectifier; (a) electrolyzer side $I_{\mathrm{DC}} = 9000\,\mathrm{A}$, (b) AC side $I_{\mathrm{DC}} = 9000\,\mathrm{A}$, (c) electrolyzer side $I_{\mathrm{DC}} = 1000\,\mathrm{A}$, (d) AC side $I_{\mathrm{DC}} = 1000\,\mathrm{A}$.

3.3. Simulated two-stage buck converter

The first stage of the rectifier is a 12-pulse diode bridge, which is connected to the 20 kV, 50 Hz electricity grid through a 3.9 MVA three-winding three-phase transformer, whose resistance and leakage inductance are set to 0.2% and 6%, respectively, for each winding. Starting from the primary, the

windings of the transformer are set to grounded Y, grounded Y, and D1. The line-to-line voltage RMS value of the transformer secondary windings is set to 250 V. The second stage of the rectifier is an IGBT-based buck converter with a switching frequency of 1 kHz. A 1 mF DC link capacitor is placed between the diode bridge and the buck converter, and a 96 µH inductor is selected for the buck converter output. The resulting AC and DC voltage and current waveforms with the buck converter bridge at the 9000 A and 1000 A DC current set points are presented in Fig. 5.

3.4. Simulated modular single-stage IGBT rectifier

The line-to-line voltage RMS value of the transformer secondary windings is set to 180 V because of the voltage boosting nature of the bidirectional IGBT bridges. A 3.9 MVA two-winding three-phase transformer, whose resistance and leakage inductance are set to 0.2% and 6%, respectively, for both windings, is selected with grounded Y connections. In practice, grounding the star-point of the transformer secondary may cause greater common-mode voltages and currents, which could have adverse effects on the system. The LCL filter components are selected as follows: electricity grid side inductance (from which the leakage inductance of the transformer secondary winding has been subtracted) $L_{\mathrm{grid}} = 40.2\,\mu\mathrm{H}$, converter side inductance $L_{\mathrm{con}} = 48.1\,\mu\mathrm{H}$, capacitance of the LCL filter $C_{\mathrm{f}} = 2.4\,\mathrm{mF}$, and damping resistor $R_{\mathrm{d}} = 24.3\,\mathrm{m}\Omega$. The capacitor for the IGBT module output is selected as $C_{\mathrm{out}} = 87\,\mathrm{mF}$, which results in a total output capacitance of 870 mF for the 10 parallel IGBT modules. The switching frequency of the IGBTs is 1 kHz–5 kHz depending on the total DC current required, and all the IGBT bridges aim to share the load evenly. The resulting AC and DC voltage and current

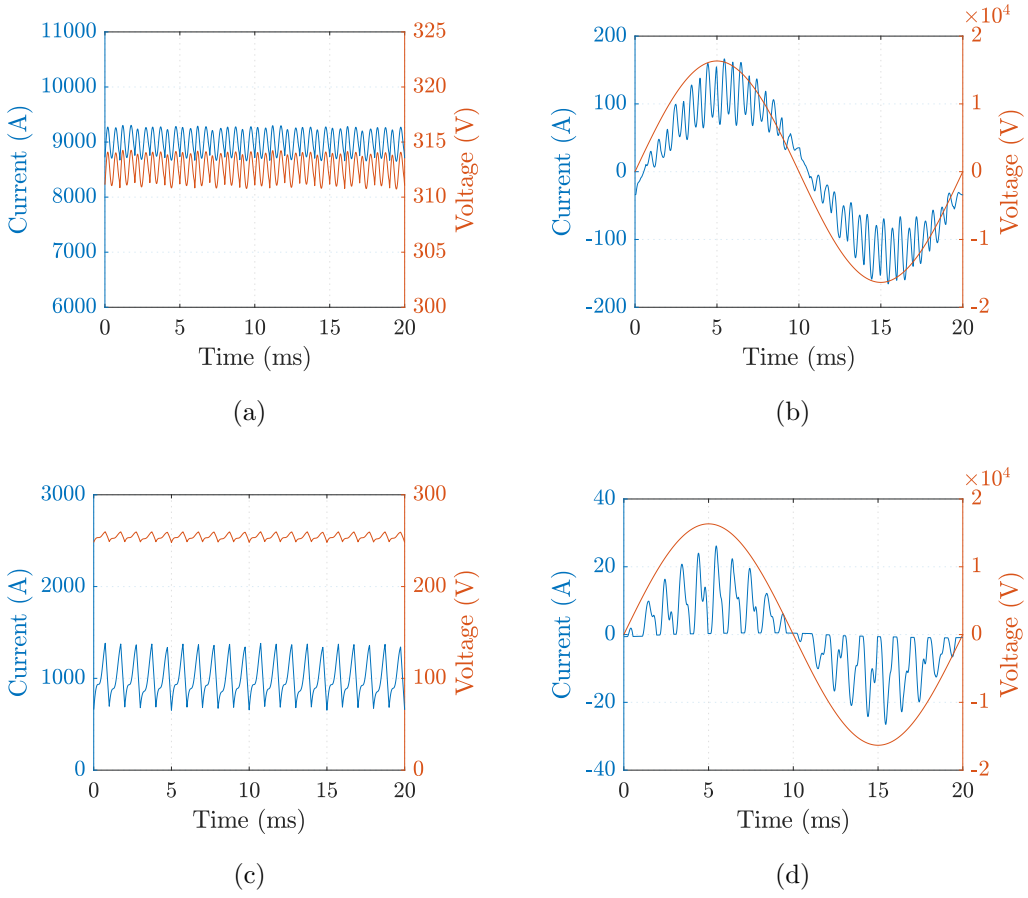

Fig. 5. Current and voltage waveforms as a function of time with the two-stage buck converter; (a) electrolyzer side $I_{\mathrm{DC}} = 9000\,\mathrm{A}$, (b) AC side $I_{\mathrm{DC}} = 9000\,\mathrm{A}$, (c) electrolyzer side $I_{\mathrm{DC}} = 1000\,\mathrm{A}$, (d) AC side $I_{\mathrm{DC}} = 1000\,\mathrm{A}$.

waveforms with the modular IGBT converter at the 9000 A and 1000 A DC current set points are illustrated in Fig. 6. At the minimum DC current set point (1000 A), the DC waveforms are close to ideal, and the RMS value of the harmonic component in the DC current waveform at the switching frequency (4.85 kHz) is only 0.05%. At the nominal load (9000 A), the switching

frequency target of 1 kHz is more prevalent in the DC current waveforms, but the current ripple is still the smallest of the investigated topologies.

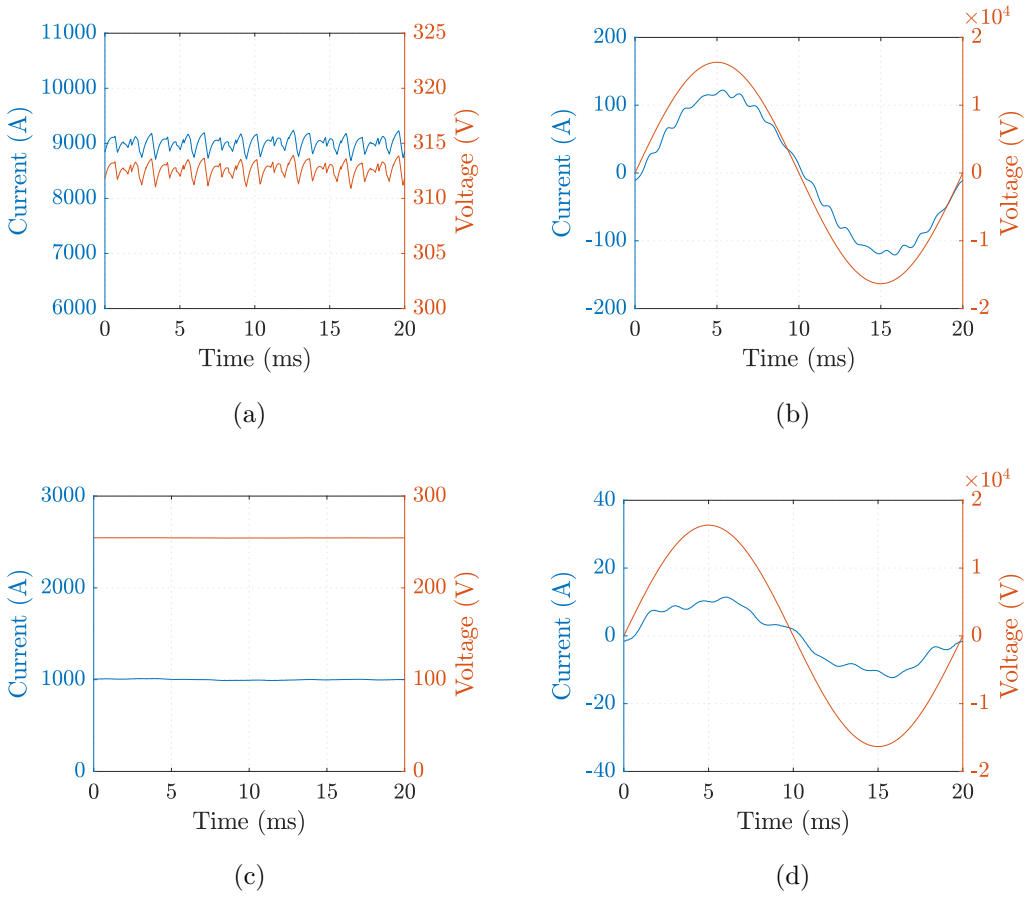

Fig. 6. Current and voltage waveforms as a function of time with the modular, single-stage, and voltage-boosting converter; (a) electrolyzer side $I_{\mathrm{DC}} = 9000\,\mathrm{A}$, (b) AC side $I_{\mathrm{DC}} = 9000\,\mathrm{A}$, (c) electrolyzer side $I_{\mathrm{DC}} = 1000\,\mathrm{A}$, (d) AC side $I_{\mathrm{DC}} = 1000\,\mathrm{A}$.

3.5. Comparison of the topologies

The DC current waveforms of each of the four investigated power supply topologies are analyzed in Table 2. For fuel cells, the switching frequency

for power electronic converters has been suggested to be greater than 1.25 kHz, and the current ripple not more than 5% to ensure normal long-term operation [25]. Minimized current ripple may also lead to a wider safe control range for the DC current mean value of the electrolyzer as the instantaneous current densities won't reach $0\,\mathrm{A\,cm^{-2}}$ even at lower DC current set points. The recommended specification for current ripple can only be met by the two-stage buck rectifier topology closer to nominal load, and the modular single-stage IGBT rectifier topology at all the studied DC current set points. With the modular single-stage IGBT rectifier at the minimum DC current set point (1000 A), the most dominant AC component in the DC current is at 50 Hz, not at the switching frequency of 5 kHz; at the nominal load (9000 A), the switching frequency of 1 kHz produces the most dominant harmonic amplitude to the DC current waveform.

The SEC for the water electrolyzer stack, the DC side power factor, and the AC side power factor with the four power supply topologies are presented in Fig. 7. The transistor-based topologies show a considerably smaller current ripple on the DC side than the purely thyristor-based topologies, which leads to a reduced SEC of the water electrolyzer with the transistor-based topologies. The modular single-stage IGBT rectifier topology is able to achieve up to 4.5%, 1.5%, and 0.1% lower SEC of the water electrolyzer stack than with the 6-pulse thyristor bridge, the 12-pulse thyristor bridge, and the two-stage buck converter solution, respectively. The difference in the SEC is highest at partial loads as studied in [15], but the benefit of transistor-based rectifiers is not as significant as previously reported because of the presence of the leakage inductance of the transformer and a more accurate nonlinear

stack model applied in this study. However, the AC voltage level must be optimally selected for the thyristor topologies, because if the AC voltage is unnecessarily high, the thyristors have to operate at higher firing angles. An on-load tap changer (OLTC) is then required to adjust the AC voltage level optimal for the thyristors especially over the lifetime of the electrolytic cell stack when the stack voltage level continuously increases as a result of voltage degradation.

OLTCs cannot eliminate the reactive power in thyristor bridge topologies. The significant DC current ripple caused by thyristor and diode rectifiers leads to a poor power factor. The AC power factor $\cos\phi_{\mathrm{AC}}$ with the 6-pulse thyristor is 0.530–0.895 in the studied DC current set point range, while the 12-pulse thyristor improves the AC power factors to 0.638–0.907 (Fig. 7c). The two-stage buck converter topology improves the AC power factor further to 0.796–0.947, but still, the power factor stays far from optimal. With the modular single-stage IGBT rectifier, the power factor can be controlled, which results in $0.988 \leq \cos\phi_{\mathrm{AC}} \leq 0.999$ in the DC current set point range, when the target power factor for control is 1. Reactive power compensation equipment and/or operational costs for reactive power allowance are thus required with all the rectifier topologies under study except for the modular single-stage IGBT rectifier. The distribution of the power components with the four power supplies is illustrated in Fig. 8. With all four topologies, the distortion component of the reactive power Q_{D} is more dominant than the phase shift component Q_{S}, but only with the modular single-stage IGBT rectifier the reactive power is, on the whole, low enough for electricity grid operation on a large scale.

	6p thyristor		12p thyristor		Two-stage buck		Modular IGBT	
	1 kA	9 kA	1 kA	9 kA	1 kA	9 kA	1 kA	9 kA
Min. current (A)	1.2	6790	5.6	7973	652	8651	989	8687
Max. current (A)	2615	10488	1671	9529	1383	9303	1012	9238
Current ripple (%)	100	13	56	5	16	2	0.5	0.8
Frequency (Hz)	300	300	600	600	1000	2000	50	1150

Table 2. Minimum and maximum instantaneous DC current values of the investigated power supply topologies at the minimum and maximum DC current set points under study. Current ripple (%) describes the ratio of the RMS value of the dominating current harmonic component to the DC component. Frequency indicates the frequency of the dominating harmonic component in the DC current waveform.

The resulting annual energy consumption of the water electrolyzer with the four power supply solutions is analyzed according to the load profiles presented in Table 1. With the real industrial load profile (a) presented in Table 1, the modular single-stage IGBT rectifier topology is able to achieve 0.6%, 0.04%, and 0.02% lower annual energy consumption of the water electrolyzer stack than with the 6- and 12-pulse thyristor bridges and with the buck converter solution, respectively. With the load profile (b) with higher shares of solar PV and wind power production presented in Table 1, the respective benefits in annual stack energy consumption are 2.1%, 0.3%, and 0.04%, when all topologies are assumed to be able to safely operate the electrolyzer at low partial loads. Alternatively, the electrolyzer can operate in a hybrid mode supplied by the electricity grid and curtailed power from renewable energy sources. Assuming the annual hydrogen production equal in the grid operation case, the energy saving potential of the modular single-

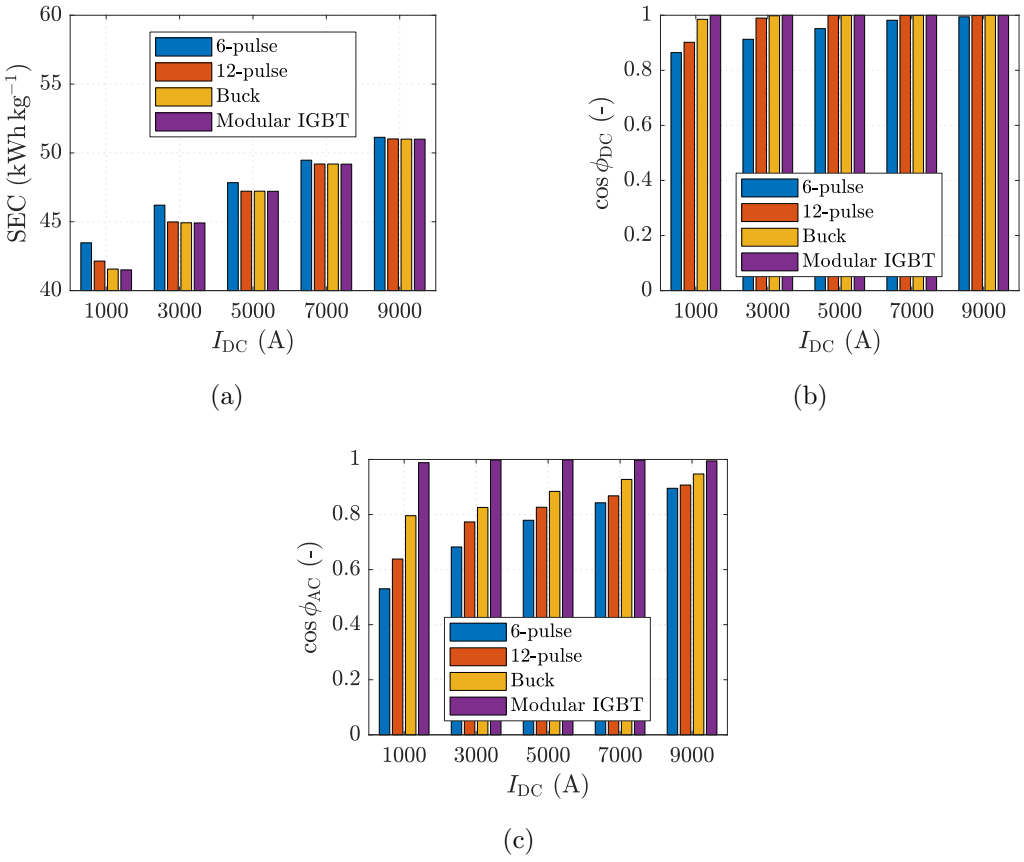

Fig. 7. Comparison of the power supply with the 3 MW alkaline water electrolyzer; (a) SEC, (b) DC side power factor, (c) AC side power factor.

stage IGBT solution is 1.2%, 0.08%, and 0.02% compared with the other topologies under study. However, the benefit of improved power quality with transistor-based topologies may be higher in renewable power production - based operation if poor DC power quality restricts prolonged operation at low partial loads in practice: thyristor-based power supplies may encounter system shutdowns due to dangerously high volume fractions of hydrogen gas in the oxygen gas outlet of the electrolyzer at low partial loads caused by the

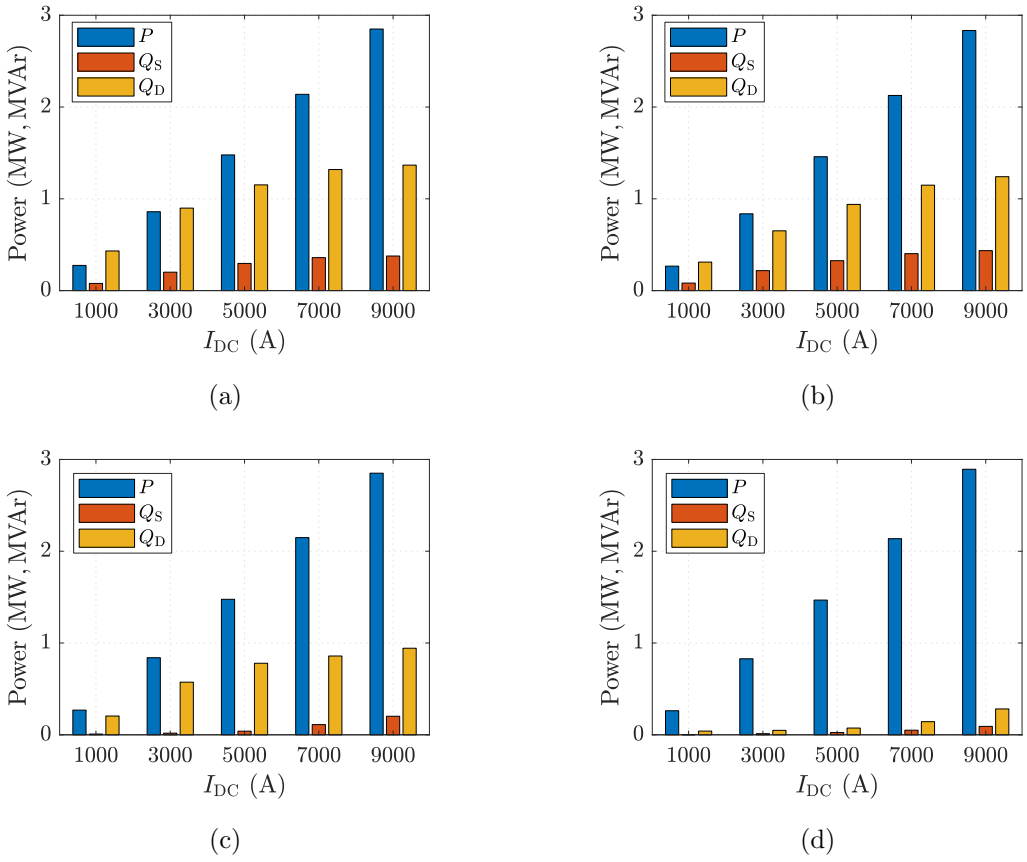

Fig. 8. Comparison of the power components on the AC side; (a) 6-pulse thyristor bridge, (b) 12-pulse thyristor bridge, (c) 12-pulse diode bridge followed by a buck converter, (d) modular IGBT.

instantaneous current approaching 0 A.

3.6. Economic analysis

Rectifier costs were estimated on the basis of the recent MW-scale equipment purchase history of the Electrical Machines Laboratory of Lappeenranta–Lahti University of Technology LUT, as well as on direct price requests from the power supply manufacturers. The baseline estimate for the four rec-

tifier topologies in EUR/A is then used to calculate the solution costs in EUR/kVA. The conversion from EUR/A to EUR/kVA takes into account the power factor and line-to-line voltage level at the transformer secondary for each topology. Transformer, filter, and reactive power compensation component prices were also considered in order to make a more comprehensive economic comparison [26, 27].

Reactive power compensation can be active and/or passive, and active compensation equipment may be as much as five times more expensive than the passive compensation equipment. Here, 40 EUR/kVAr and 130 EUR/kVAr are assumed for passive and active compensation equipment, respectively. To optimize the AC power factor at all the DC current set points, the passive compensation was dimensioned according to the mean value between the minimum ($Q_{\min}$) and maximum ($Q_{\max}$) reactive power totals among the operating points (1000 A–9000 A), and the required active compensation according to half of the difference $Q_{\max} - Q_{\min}$.

Cost estimation of the studied rectifier topologies in relation to output current and power is presented in Table 3. The two-stage topology has the highest CAPEX as the solution employs a DC/DC buck converter in addition to the 12-pulse bridge while still requiring the installation of reactive power compensation equipment. The modular single-stage IGBT rectifier is the only solution that can eliminate costs related to reactive power compensation. However, the overall cost of the modular IGBT topology remains significantly higher than the thyristor topologies' due to the highest relative difference between the electric current and voltage in the transformer secondary. The baseline EUR/A cost for the IGBT bridge modules originates

from hardware that has notably different ratings for electric current and voltage, and from the lower line-to-line voltage in the transformer secondary required by the voltage-boosting nature of the IGBT bridges. Therefore, the EUR/kVA cost estimate for the modular single-stage IGBT topology may be higher than a proper system design would yield. The estimated investment cost of the IGBT rectifier modules (0.102 EUR/VA) is more than double the current price of centralized PV inverters, which is 0.04 EUR/W [28]. The overall solution cost for the modular single-stage IGBT solution is also much higher than the centralized solar PV inverter system cost of 0.07 EUR/W–0.09 EUR/W in Germany in 2019 [28]. However, the modular IGBT topology benefits from the extensive use of similar power electronic converters in the rapidly growing renewable power production system markets. For example, the solar inverter price has been found to be as low as 0.025 EUR/W in 2019 and to follow an assumed learning rate of 15%–25% for investment cost decrease [29]. In order to reach the cost level of centralized solar PV inverter systems with the modular single-stage IGBT rectifier in MW-scale electrolysis applications, the DC voltage for the water electrolyzer stack (assembly) should be increased to lower the relatively high electric currents.

The reactive power compensation can be implemented by having the active and passive compensation equipment installed by the electrolytic hydrogen producer or by financial compensation to the distribution system operator at a specified tariff according to the provided reactive power compensation volume (EUR/kVAr). In recent years, the issue of reactive power compensation has become more acute. In order to ensure energy security, transmission system operators systematically raise tariffs, thus forcing cus-

tomers to install compensation equipment [30]. As can be seen from the cost analysis (Table 4, 3 MW 10 kA DC electrolysis application), investing in own equipment is financially justified under current conditions. However, it should be noted that even optimal reactive power compensation equipment does not solve the issue caused by the mismatch between electric current and voltage waveforms from the transformer to the water electrolyzer stack, the increase in apparent power.

Alkaline water electrolyzer stacks have a typical lifetime of 60 000 h–90 000 h, and the cell stack may contribute to half of the investment cost of an water electrolysis plant [31]. The effect of DC power quality on the lifetime of electrolyzers remains unquantified, but the maximum 5% current ripple and the minimum switching frequency of 1.25 kHz have been recommended for fuel cells [25]. Pourbaix diagrams can be essential in further detailed analysis on the possible effects power quality may have on water electrolyzers. The cell voltages may remarkably vary according to the fluctuations caused by the operation of the power semiconductor devices, depending on the impedances present in the circuit and the switching frequency used. In other words, high amplitude current harmonics excited by low frequency switching, e.g., < 1.25 kHz, may force the cell voltage potential to a thermodynamically undesirable phase region, and thus poor power quality may accelerate degradation in an electrolytic cell. This phase region analysis would always be specific to the water electrolysis technology, material selection, and operating conditions [32]. In Fig. 3, the stack voltage is able to follow the 300 Hz current fluctuations, and therefore low frequency harmonics may contribute to accelerated cell degradation and corresponding increased

cell overpotentials. For PEM water electrolyzers, voltage cycling on the time scale of seconds has been shown to contribute to accelerated performance decrease [33].

In addition to the lifetime of electrolytic cells, it is important that the power supply to them is both reliable and optimal in terms of energy efficiency. Thyristor- and diode-based topologies are well-known for their reliability, and lifetimes exceeding even 30 years have been reported in certain applications [34]. Still, thyristor- and diode-based topologies are not immune to wear and tear [12]. The two-stage topology—a 12-pulse diode bridge followed by a buck converter—adds a DC/DC conversion stage with parallel IGBT switches, and is thus more likely to result in higher maintenance costs and decreased reliability compared with the single-stage topologies based on only thyristors and/or diodes. Both the thyristor bridge topologies and the two-stage topology require reactive power compensation equipment, which requires regular maintenance. The modular single-stage topology based on IGBT modules employs a similar power electronic converter solution as typically seen in wind turbines and centralized solar PV plants; these power converter solutions have a design lifetime of 20–30 years, but require regular maintenance or even module replacements [35]. The solar and wind power applications set a more demanding operation regime than grid-connected water electrolysis, and therefore, the design lifetime of 20–30 years should be achievable for the modular IGBT rectifier topology also in electrolytic hydrogen production. In terms of reliable continuous operation, the modular IGBT solution may strongly benefit from the possibility to operate uninterrupted even when a single module fails: failed module would be discon-

	6p thyristor	12p thyristor	Two-stage buck	Modular IGBT
Rectifier, EUR/A	18	19	48	32
Rectifier, EUR/kVA	42	44	111	101.9
	$\cos\phi = 0.90$	$\cos\phi = 0.92$	$\cos\phi = 0.96$	$\cos\phi = 0.99$
	$I_{\mathrm{AC}} = 7698\,\mathrm{A}$	$I_{\mathrm{AC}} = 7531\,\mathrm{A}$	$I_{\mathrm{AC}} = 7217\,\mathrm{A}$	$I_{\mathrm{AC}} = 9720\,\mathrm{A}$
	$U_{\mathrm{AC}} = 250\,\mathrm{V}$	$U_{\mathrm{AC}} = 250\,\mathrm{V}$	$U_{\mathrm{AC}} = 250\,\mathrm{V}$	$U_{\mathrm{AC}} = 180\,\mathrm{V}$
	$P = 3000\,\mathrm{kW}$	$P = 3000\,\mathrm{kW}$	$P = 3000\,\mathrm{kW}$	$P = 3000\,\mathrm{kW}$
	$\lvert S\rvert = 3333\,\mathrm{kVA}$	$\lvert S\rvert = 3261\,\mathrm{kVA}$	$\lvert S\rvert = 3125\,\mathrm{kVA}$	$\lvert S\rvert = 3030\,\mathrm{kVA}$
Transformer, EUR/kVA	13	14.4	14.4	13
Filter, EUR/kVA			inductor 7.8 capacitor 1.3	LCL 33.1 capacitor 5.6
Passive compensation, EUR/kVA	11.1	10	7.6	0
Active compensation, EUR/kVA	19.1	19.8	16.1	0
Total cost, EUR/kVA	85.2	88.2	158.2	153.6

Table 3. Power supply cost evaluation comparing the four rectifier topologies in a 3 MW, 10 kA electrolysis application.

nected from the system, and the electrolytic gas production would continue with possibly limited maximum electrolyzer stack power. The growing power electronic converter markets in renewable power generation and the price decrease in PWM-controlled power electronic converter modules support the cost competitiveness over the design lifetime of the application. In addition, the modular IGBT topology does not require any compensation equipment, passive or active, and associated maintenance costs. Active compensation equipment may consist of similar power electronic converters as the modular single-stage IGBT topology itself.

3.7. Discussion

All the investigated power supply topologies would benefit from a higher DC voltage level of the electrolytic cell stack assembly. From the medium

	6p thyristor	12p thyristor	Two-stage buck	Modular IGBT
Reactive power, compensation equipment cost, EUR	100 789	97 283	74 098	0
Annual cost of reactive power, EUR	70 825	65 017	47 932	0

Table 4. Reactive power compensation cost evaluation comparing the three rectifier topologies. 4 EUR/kVAr is assumed for the price of reactive power allowance.

voltage grid transformer to the electrolyzer, the electric currents would be lower resulting in lower losses in the transformer secondary and busbars. The proposed stack voltage increase would be crucial for the modular single-stage IGBT topology as it is voltage-boosting in nature, and thus requires a relatively lower AC voltage level to operate. The higher electric current may also limit the efficiency of the modular IGBT supply solution itself.

Thyristors generally have a higher efficiency than IGBT switches. However, to meet the increasing demand of DC current supply for an electrolyzer system, the thyristor bridges may have to be split among multiple transformer secondaries to share the currents and to minimize losses in the semiconductor devices. This current sharing may be done even with a 6-pulse thyristor bridge by selecting ANSI 45 configuration instead of the ANSI 25 illustrated in Fig. 1a, in other words, to have two Y-connected transformer secondaries to form the 6-pulse thyristor rectifier structure [12]. The modular IGBT topology can be configured to have multiple parallel IGBT bridges behind a single transformer secondary, which may result in a less complex and less costly transformer configuration in high-current applications.

The modular single-stage IGBT rectifier can also minimize the reactive power component, which leads to an optimized flow of electric current as the

electric current does not have to increase to compensate (i.e., to ensure the required flow of active electrical energy) the mismatch seen in the current and voltage waveforms with thyristor and/or diode bridges. Furthermore, the harmonic losses in the transformer will be reduced with the optimal power quality, and the transformer can be designed for a lower rated power when the difference between active and apparent power is minimal.

4. Conclusions

The OPEX and CAPEX costs of four power supply topologies for an industrial 3 MW alkaline water electrolyzer were studied. For purely thyristor- and/or diode-based topologies, the rectification causes significant current harmonics on both the AC and DC sides of the rectifier. The current harmonics lead to additional losses in the water electrolyzer stack and decrease the power factor. The decreased AC power factor can be compensated with reactive power compensation equipment, but the issue of power quality remains as reactive power is not eliminated in the system. Considering the four topologies under study, only the novel modular single-stage IGBT rectifier is able to optimize the power quality to the electrolyzer and the electricity grid, and thus minimize the losses in the power supply. The modular IGBT topology offers up to 4.5% lower SEC of the electrolyzer stack than the 6-pulse thyristor bridge, and up to 1.5% lower consumption than the 12-pulse thyristor bridge. The SEC with the modular IGBT topology is up to 0.1% lower than with the two-stage buck converter topology, but the two-stage topology cannot eliminate the reactive power issue and holds the highest total investment cost. Only the modular single-stage IGBT rectifier is able to reach

the power quality recommendations (>1.25 kHz switching frequency, <5% current ripple) suggested for electrolytic cells to ensure long-term operation. Furthermore, the modular IGBT topology may enable the widest safe control range for the electrolyzer DC current mean value as the current ripple is minimized; thyristor-based power supplies may have limited capabilities to safely power the electrolyzer if partial load operation is emphasized. For the investigated application, the modular single-stage IGBT rectifier could be a comparable alternative to the traditional thyristor rectifier topologies in terms of power supply investment cost especially with an increased water electrolyzer stack assembly voltage. The modular transistor-based topologies may become even more cost-competitive with emerging new power semiconductors based on SiC and/or GaN, which decrease switching losses and enable higher switching frequencies and, in turn, smaller filter components.

Acknowledgements

The authors are grateful for the Business Finland *Modular power electronics for electrolysis applications (ELPSU)* project funding 1361/31/2019.

References

[1] M. Allen, H. de Coninck, O. Dube, O. Hoegh-Guldberg, D. Jacob, K. Jiang, A. Revi, J. Rogelj, J. Roy, D. Shindell, W. Solecki, M. Taylor, P. Tschakert, H. Waisman, S. A. Halim, P. Antwi-Agyei, F. Aragón-Durand, M. Babiker, P. Bertoldi, M. Bindi, S. Brown, M. Buckeridge, I. Camilloni, A. Cartwright, W. Cramer, P. Dasgupta, A. Diedhiou, R. Djalante, W. Dong, K. Ebi, F. Engelbrecht, S. Fifita, J. Ford, P. Forster, S. Fuss, V. Ginzburg, J. Guiot, C. Handa, B. Hayward, Y. Hijioka, J.-C. Hourcade, S. Humphreys, M. Kainuma, J. Kala, M. Kanninen, H. Kheshgi, S. Kobayashi, E. Kriegler, D. Ley, D. Liverman, N. Mahowald, R. Mechler, S. Mehrotra, Y. Mulugetta, L. Mundaca, P. Newma, C. Okereke, A. Payne, R. Perez, P. Pinho, A. Revokatova, K. Riahi, S. Schultz, R. Séférian, S. Seneviratne, L. Steg, A. S. Rodriguez, T. Sugiyama, A. Thomas, M. Vilariño, M. Wairiu, R. Warren, K. Zickfeld, G. Zhou, Technical Summary, in: V. Masson-Delmotte, P. Zhai, H.-O. Pörtner, D. Roberts, J. Skea, P. Shukla, A. Pirani, W. Moufouma-Okia, C. Péan, R. Pidcock, S. Connors, J. Matthews, Y. Chen, X. Zhou, M. Gomis, E. Lonnoy, T. M. M. Tignor, T. Waterfield (Eds.), Global Warming of 1.5 °C. An IPCC Special Report on the impacts of global warming of 1.5 °C above pre-industrial levels and related global greenhouse gas emission pathways, in the context of strengthening the global response to the threat of climate change, sustainable development, and efforts to eradicate poverty, 2018, In Press.

URL `https://www.ipcc.ch/site/assets/uploads/sites/2/2019/`

02/SR15_TS_High_Res.pdf

[2] C. Chardonnet, L. De Vos, F. Genoese, G. Roig, F. Bart, T. De Lacroix, T. Ha, B. Van Genabet, Final Report: Study on early business cases for H2 in energy storage and more broadly power to H2 applications, 2017.
URL https://www.fch.europa.eu/sites/default/files/P2H_Full_Study_FCHJU.pdf

[3] The Fuel Cells and Hydrogen Joint Undertaking (FCH JU), Hydrogen roadmap Europe: A sustainable pathway for the European energy transition, 2019.
URL https://www.fch.europa.eu/publications/hydrogen-roadmap-europe-sustainable-pathway-european-energy-transition

[4] A. Buttler, H. Spliethoff, Current status of water electrolysis for energy storage, grid balancing and sector coupling via power-to-gas and power-to-liquids: A review, Renewable and Sustainable Energy Reviews 82 (2018) 2440–2454.

[5] A. Mayyas, M. Wei, G. Levis, Hydrogen as a long-term, large-scale energy storage solution when coupled with renewable energy sources or grids with dynamic electricity pricing schemes, International Journal of Hydrogen Energy 45 (33) (2020) 16311–16325.

[6] M. Carmo, D. L. Fritz, J. Mergel, D. Stolten, A comprehensive review

on PEM water electrolysis, International Journal of Hydrogen Energy 38 (12) (2013) 4901–4934.

[7] Frontier Economics, International aspects of a Power-to-X roadmap: a report prepared for the World Energy Council Germany, [Accessed: 12-Dec-2019]. (2018).
URL https://www.frontier-economics.com/media/2646/20181018_frontier_wec_germany_ptxroadmap_full-study-english.pdf

[8] M. Ram, D. Bogdanov, A. Aghahosseini, S. A. Oyewo, M. Child, U. Caldera, K. Sadovskaia, J. Farfan, L. S. Barbosa, M. Fasihi, S. Khalili, B. Dalheimer, G. Gruber, T. Traber, F. D. Caluwe, H.-J. Fell, C. Breyer, Global energy system based on 100% renewable energy — power, heat, transport, and desalination sectors, in: Study by Lappeenranta University of Technology and Energy Watch Group, Lappeenranta, Berlin, 2019.

[9] The European Commission, Communication from the commission to the European parliament, the council, the European economic and social committee and the commitee of the regions—A hydrogen strategy for a climate-neutral Europe (2020).
URL https://ec.europa.eu/energy/sites/ener/files/hydrogen_strategy.pdf

[10] G. Zhao, M. R. Kraglund, H. L. Frandsen, A. C. Wulff, S. H. Jensen, M. Chen, C. R. Graves, Life cycle assessment of H_2O electrolysis tech-

nologies, International Journal of Hydrogen Energy 45 (43) (2020) 23765–23781.

[11] J. R. Rodriguez, J. Pontt, C. Silva, E. P. Wiechmann, P. W. Hammond, F. W. Santucci, R. Alvarez, R. Musalem, S. Kouro, P. Lezana, Large current rectifiers: State of the art and future trends, IEEE Transactions on Industrial Electronics 52 (3) (2005) 738–746.

[12] J. Solanki, N. Fröhleke, J. Böcker, A. Averberg, P. Wallmeier, High-current variable-voltage rectifiers: state of the art topologies, IET Power Electronics 8 (6) (2015) 1068–1080.

[13] A. Ursúa, L. Marroyo, E. Gubía, L. M. Gandía, P. M. Diéguez, P. Sanchis, Influence of the power supply on the energy efficiency of an alkaline water electrolyser, Internationa Journal of Hydrogen Energy 34 (8) (2009) 3221–3233.

[14] Z. Dobó, Á. B. Palotás, Impact of the current fluctuation on the efficiency of Alkaline Water Electrolysis, International Journal of Hydrogen Energy 42 (9) (2017) 5649–5656.

[15] J. Koponen, V. Ruuskanen, A. Kosonen, M. Niemelä, J. Ahola, Effect of converter topology on the specific energy consumption of alkaline water electrolyzers, IEEE Transactions on Power Electronics 34 (7) (2019) 6171–6182.

[16] F.-W. Speckmann, S. Bintz, K. P. Birke, Influence of rectifiers on the energy demand and gas quality of alkaline electrolysis sys-

tems in dynamic operation, Applied Energy 250 (2019) 855–863. doi:https://doi.org/10.1016/j.apenergy.2019.05.014.

[17] F.-W. Speckmann, D. Keiner, K. P. Birke, Influence of rectifiers on the techno-economic performance of alkaline electrolysis in a smart grid environment, Renewable Energy 159 (2020) 107–116.

[18] J. Solanki, N. Fröhleke, J. Böcker, Implementation of hybrid filter for 12-pulse thyristor rectifier supplying high-current variable-voltage DC load, IEEE Transactions on Industrial Electronics 62 (8) (2015) 4691–4701. doi:10.1109/TIE.2015.2393833.

[19] V. Ruuskanen, J. Koponen, A. Kosonen, M. Niemelä, J. Ahola, A. Hämäläinen, Power quality and reactive power of water electrolyzers supplied with thyristor converters, Journal of Power Sources 459 (2020) 228075. doi:https://doi.org/10.1016/j.jpowsour.2020.228075.

[20] M. Liserre, F. Blaabjerg, S. Hansen, Design and control of an LCL-filter-based three-phase active rectifier, IEEE Transactions on Industry Applications 41 (5) (2005) 1281–1291.

[21] S. Ogasawara, J. Takagaki, H. Akagi, A. Nabae, A novel control scheme of a parallel current-controlled PWM inverter, IEEE Transactions on Industry Applications 28 (5) (1992) 1023–1030.

[22] Kun Xing, F. C. Lee, D. Borojevic, Zhihong Ye, S. Mazumder, Interleaved PWM with discontinuous space-vector modulation, IEEE Transactions on Power Electronics 14 (5) (1999) 906–917.

[23] L. Asiminoaei, E. Aeloiza, P. N. Enjeti, F. Blaabjerg, Shunt active-power-filter topology based on parallel interleaved inverters, IEEE Transactions on Industrial Electronics 55 (3) (2008) 1175–1189.

[24] V. Ruuskanen, J. Koponen, A. Kosonen, M. Hehemann, R. Keller, M. Niemelä, J. Ahola, Power quality estimation of water electrolyzers based on current and voltage measurements, Journal of Power Sources 450 (2020) 227603. doi:https://doi.org/10.1016/j.jpowsour.2019.227603.

[25] P. Thounthong, B. Davat, S. Rael, P. Sethakul, Fuel cell high-power applications, IEEE Industrial Electronics Magazine 3 (1) (2009) 32–46.

[26] L. Laaksonen, Kompensointilaitteiden vaikutus allaspumppaamon muuntamon sähkön laatuun ja loistehomaksuihin [The effect of compensation devices to the pool pumping substation's power quality and reactive power costs], Master of Science Thesis, Tampere University of Technology, 2018.

[27] Energiavirasto, Verkkokomponentit, yksikköhinnat (alv 0 %) ja pitoajat vuosille 2016–2023 [Network components, unit prices (VAT 0%) and lifetimes for years 2016–2023], [Accessed: 13-Oct-2020].
URL https://energiavirasto.fi/documents/11120570/12766832/Verkkokomponentit-ja-yksikk\%C3\%B6hinnat-2016-2023.xlsx/7bd40be6-7486-fa81-fbef-3363c71d008e

[28] Fraunhofer Institute for Solar Energy Systems, ISE with support of PSE Projects GmbH, Photovoltaics report, 2020.

URL https://www.ise.fraunhofer.de/de/veroeffentlichungen/studien/photovoltaics-report.html

[29] E. Vartiainen, G. Masson, C. Breyer, D. Moser, E. Román Medina, Impact of weighted average cost of capital, capital expenditure, and other parameters on future utility-scale PV levelised cost of electricity, Progress in Photovoltaics: Research and Applications 28 (6) (2020) 439–453. arXiv:https://onlinelibrary.wiley.com/doi/pdf/10.1002/pip.3189, doi:10.1002/pip.3189.

[30] Fingrid, Supply of reactive power and maintenance of reactive power reserves, [Accessed: 13-Oct-2020].
URL https://www.fingrid.fi/en/grid/grid-connection-agreement-phases/supply-of-reactive-power-and-maintenance-of-reactive-power-reserves/

[31] L. Bertuccioli, A. Chan, D. Hart, F. Lehner, B. Madden, E. Standen, Study on development of water electrolysis in the EU, Final report in fuel cells and hydrogen joint undertaking, 2014.

[32] M. Schalenbach, A. Zeradjanin, O. Kasian, S. Cherevko, K. Mayhofer, A perspective on low-temperature water electrolysis — challenges in alkaline and acidic technology, International Journal of Electrochemical Science 13 (2018) 1173–1226.

[33] S. M. Alia, S. Stariha, R. L. Borup, Electrolyzer durability at low catalyst loading and with dynamic operation, Journal of The Electrochemical Society 166 (15) (2019) F1164–F1172. doi:10.1149/2.0231915jes.

[34] J. Przybilla, J. Dorn, R. Barthelmess, U. Kellner-Werdehausen, H. . Schulze, F. . Niedernostheide, Diodes and thyristor —– past, presence and future, in: 2009 13th European Conference on Power Electronics and Applications, 2009,

[35] H. Wang, M. Liserre, F. Blaabjerg, P. de Place Rimmen, J. B. Jacobsen, T. Kvisgaard, J. Landkildehus, Transitioning to physics-of-failure as a reliability driver in power electronics, IEEE Journal of Emerging and Selected Topics in Power Electronics 2 (1) (2014) 97–114.